TRANSFER FUNCTION-BASED MICROSATELLITE ATTITUDE CONTROL MODEL

Ajiboye, A. T.*, Opadiji, J. F. and Popoola, J. O.

Department of Computer Engineering, Faculty of Engineering and Technology, University of Ilorin, Ilorin, Kwara State, Nigeria

*Corresponding email: ajiboye.at@unilorin.edu.ng

ABSTRACT

The oversimplification of existing transfer function models used in literature results in inadequate characterisation of microsatellite Attitude Control System, hence the need to develop a transfer function-based Systems dynamics model that adequately characterise the system. The first step in the development of an Attitude Control System for a satellite is the modelling of its dynamics. The modelling is usually carried out using the state-space approach due to the nonlinear nature of satellite Attitude Control Systems dynamics. The mathematical expressions of the satellite structure dynamic accelerating torque about its three axes were presented in this study. The actuator model was based on the dynamic model of the Brushless DC motor under the wheel loading. A linear amplifier with a first-order transfer function model was proposed to reduce the effects of sudden changes in motor speed. Proportional – Integral – Derivative controller was also proposed in this study. The responses of the subsystems and overall system to unit step function were simulated. The simulation results show that the uncompensated system was open-loop unstable, while it was closed-loop stable with rise time and settling time of 2.21s and 3.98s, respectively for all the three axes. The corresponding values of Percentage Overshoot and steady error are both zero.

Keywords: Actuator dynamics, Microsatellite attitude, PID controller, Reaction wheel, Transfer function

1 INTRODUCTION

The environment that surrounds the satellite in space contains disturbances that normally affect its attitude [1]. Therefore, there is a need to find a way of mitigating these negative effects. There are two major methods normally applied to achieve satellite attitude control. The first is the passive control method which normally utilizes space natural phenomena and satellite geometry while the second is the active control method which involves the control of satellite attitude about its axes using actuators. Despite all disturbances in the space environment, a good Attitude Control Systems (ACS) should provide the satellite with the capability of high maneuverability, high pointing stability and attitude accuracy [2]. This is to ensure that all the necessary earth pointing pay-loads can point to the desired locations on the earth surface [3]. To achieve this, the satellite needs an ACS capable of applying the necessary control torques via actuators. The first step in the development of satellite ACS is the modelling of the system dynamics. Due to the nonlinear nature of the satellite attitude control dynamics, the modelling is always carried out using Multiple Inputs Multiple Outputs (MIMO) approach whereby state space will be the only design and analysis method. This approach is more complex compared to the Single Input Single Output (SISO) method which employs transfer function as a means of system design and analysis. Based on the definition of rigid-body reference frame with origin at the centre of mass of microsatellite, formulation of Euler's equations of motion for microsatellite and substitution of gravity gradient torque into the formulated equations assuming zero model uncertainties [4] expressed the attitude dynamic model of microsatellite in state-space form. Using the inertial fixed reference coordinate, orbital coordinate reference and body-fixed reference frame, satellite ACS model was developed in terms of Euler angles and quaternion [5]. The

inertial frame and body-fixed frame unit quaternion representation were used to model the attitude of spacecraft [6]. In [7], spacecraft was modelled as a rigid body with the three actuators that supply the torques about the roll, yaw and pitch axes defines a body-fixed frame. This was achieved by using mathematical descriptions of the attitude orientation of the spacecraft in the body frame with respect to the inertial frame with a unit quaternion. By integrating the satellite and actuator dynamics together with the attitude determination and external interface models [8] developed a Simulink-based attitude determination and control model. Euler equation was used by [9, 10] to model the satellite attitude motion as a rigid body under the influence of the external moment. The resulting equations were linearised with respect to the orbital reference frame, in order to be decoupled into the pitch and roll/yaw modes. More so, linearised attitude dynamics for a very small angle deviation from Local-Vertical-Local-Horizontal (LVLH) reference frame were obtained in [11, 12] by first defining the microsatellite attitude dynamics. It was achieved by fixed-body reference frame with its origin, located in the mass centre of the microsatellite which was then transformed into a LVLH and inertial reference frames with the origin at the satellite centres of mass and earth respectively. The coordinate transformation was used to facilitate the description of the attitude in terms of Euler angles. Euler equations of motion were applied by [2] for modelling the dynamics of satellite ACS in which the dynamics of the actuator has been embedded. The work was based on rigid body assumption to give control torque together with high-speed slew capability. The system kinematic equations were formulated by using modified Rodrigues parameters. A satellite structure dynamic to implement LQG for satellite attitude controller was modelled in [13] by considering the orbital and satellite frames together and parameterized the attitude using Euler's angles. In other to obtain a linear model that aids the application of linear controller design principles, a small manoeuvre angle and satellite as a rigid body was assumed. Satellite ACS based on the dynamic equations of the satellite on Euler's equations of motion for a rigid body was modelled by [14], the quaternion Kinematic equations of motion were derived in terms of the satellite's angular velocity components. Based on the linearised Euler equation of motion, [1] modelled the dynamic of a satellite using the LVLH coordinate frame as a reference. Because of the linearization, the pitch motion equation was decoupled from the coupled roll/yaw motion equation, thereby simplifying the model so that each of the axes can be handled separately using SISO control analysis and design. By applying Euler equations of motion and also assumed that the satellite body frame reference coincided with the system principal axes of inertia, the dynamics of a CubeSat was Modelled by [15]. Under this condition the products of inertia in the satellite's inertia matrix cancelled out, making the inertial matrix become a diagonal and then gives room for the treatment of the satellite control axes separately and application of SISO system analysis and design. In all the afore-mentioned satellite ACS modelling methods described, the state space was used which makes the design and analysis mathematically intensive. In [16, 17], simple mathematical models for satellite yaw ACS based on the transfer function approach were developed. However, the type of actuator used was not specified therefore the process involved in the transmission of torque and momentum from the actuator to the satellite becomes fuzzy. The assumption that the satellite structure was being driven by the DC motor directly and lumping the satellite and rotor moment of inertial together in their work will lead to model oversimplification. Also, the amplifier contains only gain in the system model, which makes it inadequate for handling sudden changes in amplifier input voltage as a result of a sudden change in the motor speed. Attitude determination was not covered in this study as it is expected to have been considered before attitude control. Application of Kalman filter and unscented Kalman filter algorithm for estimation of microsatellite attitude was fully presented in [18]. Extended Kalman filter algorithm was used in the form of software by [14] to determine nanosatellite attitude. Since satellite dynamics, actuator and controller models are the main parts of satellite ACS [14], unity feedback structure was therefore adopted in this study. An important step in the development of satellite ACS model is to develop the mathematical model for each of its subsystems and then integrate them to form the system overall dynamic model. The time-domain performance parameters (rise time (Tr), time to peak overshoot (Tp), percentage overshoot (PO), settling time (Ts) and steady-state error (Ess)) of the system response to unit step input was used to assess the developed models.

2 SYSTEM MODELLING

The block diagram of the microsatellite ACS based on the transfer function approach is as shown in Figure 1.

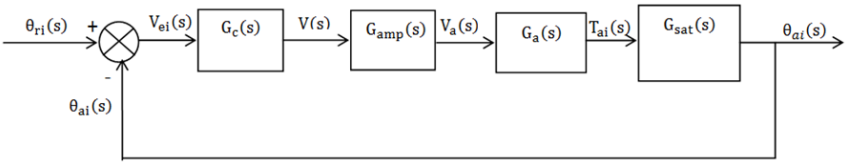

Figure 1. Satellite attitude control system block diagram

where θ_{ri} and $\theta_{ai}(s)$ are the reference attitude and actual attitude for ith axis, respectively, both in radians; V_{ei}, V and V_a are the attitude error voltage for ith axis, controller output voltage and actuator terminal voltage, respectively, all in volts; while T_{ai} is actuator output torque for ith axis in Nm; and $G_c(s)$, $G_{amp}(s)$, $G_a(s)$ and $G_{sat}(s)$ are the dynamics transfer functions of the controller, amplifier, actuator and satellite respectively. The block diagram of Figure 1 represent a closed-loop control system with unity feedback, it consists of blocks that account for the dynamics model of the controller, amplifier, actuator and satellite structure. The overall system was modelled by deriving the dynamic equation for each of the subsystems represent by each of the blocks in Figure 1 starting from satellite structure and then proceeds in backward direction to the controller stage and then find the overall system transfer function.

2.1 Modelling of Satellite Structure Dynamics

The schematic diagram of a satellite is shown in Figure 2, where the origin lies at the centre of mass (COM) of the satellite. As shown in Figure 2, the rotation about the x-, y- and z-axes represent the roll, pitch and yaw respectively. The roll-axis points in the direction of the velocity vector, the pitch-axis is perpendicular to roll and the yaw-axis points to the centre of the earth.

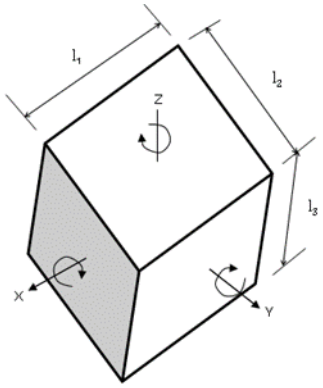

Figure 2. Schematic diagram of a microsatellite

The modelling process was started by defining the attitude of the satellite using roll, pitch and yaw angles. These three angles characterise the attitude of the satellite relative to the reference attitude. Due to compactness of the microsatellite, its attitude was determined by using the dynamics and kinematic equations, assuming that the satellite is a rigid body. The resulting satellite dynamics and kinematic equations are a set of highly coupled, nonlinear ordinary differential equations which normally requires linearisation to ease system modelling and design. According to [3] using Taylor series approximations, this equation yields the required linear model, which enables the decoupling of the 3-attitude axes into the individual axis, and thereby giving way for transfer function attitude control model development. The satellite structure dynamic accelerating torque about the roll, pitch and yaw axes, $T_{a1}(s)$, $T_{a2}(s)$ and $T_{a3}(s)$, respectively as obtained from the linear model approximation is as expressed in equation 1 [3].

$$\left.\begin{aligned} T_{a1}(s) &= -3n^2\Delta_1 J_1\theta_1(s) - n\Delta_1 J_1\omega_3(s) - s^2 J_1\theta_{a1}(s) \\ T_{a2}(s) &= 3n^2\Delta_2 J_2\theta_2(s) - s^2 J_2\theta_{a2}(s) \\ T_{a3}(s) &= -n\Delta_3 J_3\omega_1(s) - s^2 J_3\theta_{a3}(s) \end{aligned}\right\} \quad (1)$$

Where: θ_i = angular position about the i^{th}axis, J_i = i^{th} axis moment of inertial in kgm^2, $i = 1, 2, and\ 3$ for roll, pitch and yaw axes respectively, n = orbital angular velocity in rad/sec.

$$\left.\begin{aligned} \Delta_1 &= \frac{J_2 - J_3}{J_1} \\ \Delta_2 &= \frac{J_3 - J_1}{J_2} \\ \Delta_3 &= \frac{J_1 - J_2}{J_3} \end{aligned}\right\} \quad (2)$$

If the following terms $3n^2\Delta_1\theta_1(s),\ n\Delta_1\omega_3(s), 3n^2\Delta_2\theta_2(s)\ and\ n\Delta_3\omega_1(s)$ are negligible, then equation 1 becomes.

$$\left.\begin{aligned} T_{a1}(s) &= -s^2 J_1\theta_{a1}(s) \\ T_{a2}(s) &= -s^2 J_2\theta_{a2}(s) \\ T_{a3}(s) &= -s^2 J_3\theta_{a3}(s) \end{aligned}\right\} \quad (3)$$

The negative sign shows that the control torque is in opposite direction to the inertial torque. From equation 3 the satellite dynamic transfer function for roll, pitch and yaw axes is given in equation 4.

$$\left.\begin{aligned} \frac{\theta_{a1}(s)}{T_{a1}(s)} &= \frac{1}{J_1 s^2} \\ \frac{\theta_{a2}(s)}{T_{a2}(s)} &= \frac{1}{J_2 s^2} \\ \frac{\theta_{a3}(s)}{T_{a3}(s)} &= \frac{1}{J_3 s^2} \end{aligned}\right\} \quad (4)$$

Using Figure 2, the expressions for the satellite structure moment of inertial J_1, J_2 and J_3 about the roll, the pitch and the yaw axes, respectively were determined as follows:

$$\left.\begin{aligned} J_1 &= \frac{M(l_2{}^2 + l_3{}^2)}{12} \\ J_2 &= \frac{M(l_1{}^2 + l_3{}^2)}{12} \\ J_3 &= \frac{M(l_1{}^2 + l_2{}^2)}{12} \end{aligned}\right\} \quad (5)$$

Where M is mass of the satellite in kg, l_1, l_2 and l_3 are the distances in meters along the roll, pitch and yaw axes, respectively.

2.2 Modelling of Actuator Dynamic

The reaction wheel actuator is proposed in this study due to its modelling and realisation simplicity compared to moment-gyro [19]. A reaction wheel is a combination of electric motor and flywheel which can rotate freely along a given axis of a satellite [2, 19]. The motor choice is dictated by ease of control of both motor rotor position and its derivatives. As a result, the selection is usually made from the available direct current (dc) motors. But it should also be noted that BLDC motors are highly favoured due to their inherent advantages over the conventional ones [20, 21, 22]. A reaction wheel has a similar dynamic model as that of the BLDC under the wheel loading. When the motor rotates, the wheel angular momentum builds up and leads to the application of equal and opposite torques on the satellite structure about a given satellite axis. The BLDC motor exists in multiphase configurations, but the most common is that of 3-phase because of its better efficiency and good precision in control [22]. The per-phase equivalent circuit diagram of the 3-phase BLDC motor is as shown in Figure 3.

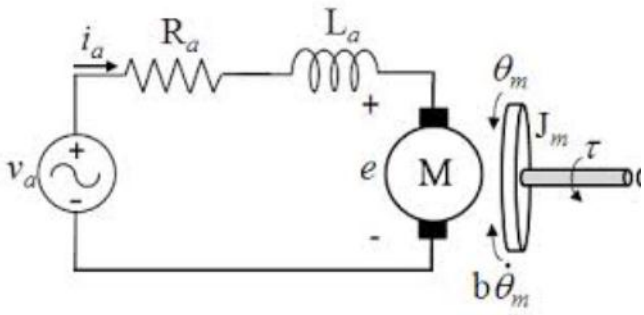

Figure 3. Per-phase equivalent circuit of brushless dc motor [23]

From Figure 3, expressing all the motor variables in s-domain and then applying Kirchhoff voltage law yields.

$$V_a(s) = I_a(s)R_a + L_a s I_a(s) + E_b(s) \quad (6)$$

Where: V_a =DC source voltage in volts, I_a = Armature current in amperes, R_a = Armature resistance in ohms, L_a = Armature inductance in henrys, E = Motor back emf in volts.

But $E_b(s) = K_b s\theta_m(s)$ (7)

Where: K_b = Motor emf constant in volt/rad/sec. The electrical torque developed by the motor is:

$$T(s) = K_m I_a(s) \quad (8)$$

Where: K_m is the motor torque constant in Nm/A. Incorporating the wheel structure into the BLDC motor load transforms the whole arrangement to reaction wheel and the mechanical torque developed by the motor under this condition is the reaction wheel torque (T_w) and is expressed as follows.

$$T_w(s) = J_m s^2\theta_m(s) + J_w s^2\theta_m + bs\theta_m(s) \quad (9)$$

Where: J_m = Motor rotor moment of inertial in kgm^2, b = Motor rotor coefficient of viscous friction in Ns/m^2, J_w =Wheel moment of inertial in kgm^2. From equation 9.

$$T_w(s) = (J_m + J_w)s^2\theta_m + bs\theta_m(s) \quad (10)$$

In practice $J_w \gg J_m$ and b is normally negligible [23] making equation 9 become equation 11.

$$T_w(s) = J_w s^2\theta_m(s) \quad (11)$$

Substituting equation 7 into equation 6 and then solving for $I_a(s)$ gives.

$$I_a(s) = \frac{V_a(s) - K_b s\theta_m(s)}{L_a s + R} \quad (12)$$

And if equation 12 is substituted into equation 8, it gives.

$$T(s) = \frac{K_m(V_a(s) - K_b s\theta_m(s))}{L_a s + R} \quad (13)$$

The transfer function of the reaction wheel is obtained by assuming that the motor electrical and mechanical torques are equal (i.e. equating equations 11 and 13), as follows:

$$\frac{\theta_m(s)}{V_a(s)} = \frac{K_m}{(L_a s + R)J_w s^2 + K_m K_b s} \quad (14)$$

Or

$$\frac{\theta_m(s)}{V_a(s)} = \frac{\frac{1}{K_b}}{\frac{J_w L_a}{K_m K_b}s^3 + \left(\frac{J_w R}{K_m K_b}\right)s^2 + s} \quad (15)$$

Expressing equation 15 in terms of reaction wheel torque, mechanical time constant (τ_m) and electrical time (τ_e) constant gives equation 16.

$$\frac{T_w(s)}{V_a(s)} = \frac{K\,J_w s}{\tau_m \tau_e s^2 + \tau_m s + 1} \tag{16}$$

Where: $K = \frac{1}{K_b}$. Negligible connecting wire resistance was assumed, therefore when the motor electrical parameters are given as line-to-line ($L - L$) value which is the common practice in the motor table of parameters, the mechanical and electrical time constants become.

$$\tau_m = 0.86 \frac{R_{a_{L-L}} J_m}{K_{b_{L-L}} K_m} \tag{17}$$

$$\tau_e = \frac{L_{a_{L-L}}}{R_{a_{L-L}}} \tag{18}$$

2.3 Selection of Reaction Wheel

Reaction wheel selection is based on its output torque, momentum storage and power consumption, therefore there is the need to develop necessary equations for determining these parameters. The relationship between the torque produced by reaction wheel and the applied torque to the satellite along a given satellite axis, assuming negligible losses is as mathematically expressed in equation 19.

$$T_{wi} = -T_{ai} \tag{19}$$

Where: T_{wi} = torque generated by reaction wheel in Nm about i axis, T_{ai} = torque applied to the satellite by the reaction wheel about i axis in Nm. By fitting the existing data from over 20 reaction wheels, [19] proposed equation 20 as the power model.

$$P_{wi} = 1000 T_{wi} + 4.51(\mathrm{h}_{wi})^{0.47} \tag{20}$$

Where: P_{wi} = power required by i axis reaction wheel in Watts, T_{wi} = magnitude of the i axis reaction wheel output torque in Nm, h_{wi} = i axis reaction wheel instantaneous momentum in Nm-sec.

But $T_{wi} = \dot{\omega_w} J_{wi} = -\dot{\omega_s} J_i$ (21)

Where: $\dot{\omega_w}$ = reaction wheel maximum angular acceleration in degree/sec/sec, $\dot{\omega_s}$ = satellite maximum angular acceleration in degree/sec/sec, J_{wi} = reaction wheel moment of inertial about i axis in kgm^2, J_i = satellite moment of inertial about i axis in kgm^2.

$$\mathrm{h}_{wi} = \omega_w J_{wi} = -\omega_s J_i \tag{22}$$

Where: ω_w is the reaction wheel angular velocity in degree/sec, ω_s is the satellite maximum slew rate in degree/sec. Therefore,

$$P_{wi} = 1000 \dot{\omega_s} J_i + 4.51(\omega_s J_i)^{0.47} \tag{23}$$

P_{wi} can be determined by substituting the value of J_i , the maximum value of $\dot{\omega_s}$ and ω_s into equation 23. For effective LEO satellite imaging, the slew rate and acceleration must be appropriately selected. The values (3 deg/sec and 1.5 deg/sec/sec) proposed by [19] were adopted in this study. Therefore, using equation 21, the required torques for the reaction wheel were 0.0164, 0.0164 and 0.0210 Nm for roll, pitch and yaw, respectively. The corresponding momenta were also determined using equation 22, and the values obtained were 0.0328, 0.0328 and 0.0419 Nm-sec. for roll, pitch and yaw, respectively. Finally, using equation 23 the powers needed by the roll, pitch and yaw reaction wheel were 17.2793, 17.2793 and 21.9756 W respectively, using. Based on the value of required wheel torque, momentum and power obtained, Maxon EC 45 flat ϕ 45 mm, 30-Watt BLDC motor with Hall sensors was selected to power the wheel. All the required motor parameters were extracted from the table of parameters and units of Maxon motor in [24]. The actuator general and specific transfer functions for roll, pitch and yaw axis were determined from equation 16 and are as shown in equations 24 and 25 respectively.

$$\frac{T_{wi}(s)}{V_a(s)} = \frac{K J_{wi} s}{\tau_m \tau_e s^2 + \tau_m s + 1} \tag{24}$$

$$\left.\begin{aligned}\frac{T_{w1}(s)}{V_a(s)} &= \frac{KJ_{w1}s}{\tau_m\tau_e s^2+\tau_m s+1}\\ \frac{T_{w2}(s)}{V_a(s)} &= \frac{KJ_{w2}s}{\tau_m\tau_e s^2+\tau_m s+1}\\ \frac{T_{w3}(s)}{V_a(s)} &= \frac{KJ_{w3}s}{\tau_m\tau_e s^2+\tau_m s+1}\end{aligned}\right\} \quad (25)$$

2.4 Modelling of Amplifier Dynamics

This sub-system is a power amplifier whose input is from Pulse Width Modulation (PWM) unit. The output power and voltage from PWM is always very small to power the BLDC motor, therefore there is the need for a power amplifier that will amplify both the voltage and power. This amplifier converts its input to a voltage that is high enough to power the motor at its output. Sudden increase or decrease in the speed of electric motor always results to high current been drawn by the motor, to ameliorate this effect a linear amplifier with a first-order transfer function of the form shown in equation 26 was proposed [21].

$$\frac{V_a(s)}{V(s)} = \frac{K_{amp}}{\tau_{amp}s+1} \quad (26)$$

Where: V_a= motor terminal voltage in volt, V= PWM input voltage in volt, K_{amp}= the gain from PWM to the motor terminal voltage (V_a), τ = amplifier time constant in sec. At steady-state:

$$V_a(s) = K_{amp}V(s) \quad (27)$$

2.5 Controller Modelling

PID controller was proposed in this study because of its advantages over other controller algorithms. The integral, proportional and derivative action takes care of the past, present and future control error respectively. From Figure 1 the relationship between the input voltage and output voltage of the controller, for PID control law is as shown in the transfer function of equation 28.

$$G_c(\mathrm{s}) = \frac{\mathrm{V(s)}}{V_{ei}(s)} = \frac{K_D s^2+K_P s+K_I}{s} \quad (28)$$

Where: K_P = Proportional gain, K_I = Integral gain, K_D = Derivative gain

2.6 Dynamic Model of the overall Microsatellite ACS

From Figure 1 the attitude error is the difference between θ_{ri} and θ_{ai}. Therefore, the relationship among V_{e1}, θ_{ri} and θ_{ai} is as expressed in equation 29.

$$V_{e1} = (\theta_{ri} - \theta_{ai}) \quad (29)$$

We are concerned with both steady-state and transient responses of the system. For the steady-state, there are two scenarios of interest, the system response when there is no attitude error (the motor is stationary) and otherwise (when the motor is moving with a constant velocity in such a direction as to reduce the attitude error to zero). To investigate the system response under these conditions, the mathematical model that relates the reference attitude and actual attitude together based on all the subsystem transfer functions was derived. This model was obtained from the block diagram of Figure 1 by combining the model of the constituent component blocks into a single model representing the overall dynamic of the ACS. To ease the process, the system open-loop transfer function was first determined then followed by the derivation of system closed-loop transfer function as follows: From equations 4, 24, 26 and 28; the system overall open-loop transfer function is as expressed in equation 30.

$$\frac{\theta_{ai}(s)}{V_{ei}(s)} = \frac{\theta_{ai}(s)}{T_{ai}(s)} \times \frac{T_{wi}(s)}{V_a(s)} \times \frac{V_a(s)}{V(s)} \times \frac{V(s)}{V_{ei}(s)} \quad (30)$$

The general open-loop transfer function for the uncompensated system was obtained by assuming $G_c(s) = 1$, that is, $K_P = 1$, $K_I = 0$, and $K_D = 0$ so that $V_{ei}(s) = V(s)$ and is as shown in equation 31.

$$\frac{\theta_{ai}(s)}{V_{ei}(s)} = \frac{A_i}{s^4+Bs^3+Cs^2+Ds} \tag{31}$$

Where: $A_i = \frac{KJ_{wi}K_{amp}}{J_i\tau_m\tau_e\tau_{amp}}$, $B = \frac{(\tau_{amp}+\tau_e)}{\tau_e\tau_{amp}}$, $C = \frac{(\tau_{amp}+\tau_m)}{\tau_m\tau_e\tau_{amp}}$, $D = \frac{1}{\tau_m\tau_e\tau_{amp}}$

From equation 31 the open-loop transfer function for roll, pitch and yaw attitude control dynamics when the system was not compensated is as shown in equation 32.

$$\left.\begin{aligned}\frac{\theta_{a1}(s)}{V_{e1}(s)} &= \frac{A_1}{s^4+Bs^3+Cs^2+Ds}\\ \frac{\theta_{a2}(s)}{V_{e2}(s)} &= \frac{A_2}{s^4+Bs^3+Cs^2+Ds}\\ \frac{\theta_{a3}(s)}{V_{e3}(s)} &= \frac{A_3}{s^4+Bs^3+Cs^2+Ds}\end{aligned}\right\} \tag{32}$$

From equation 31 the general closed-loop transfer function for the uncompensated system is as shown in equation 33.

$$\frac{\theta_{ai}(s)}{\theta_{ri}(s)} = \frac{A_i}{s^4+Bs^3+Cs^2+Ds+A_i} \tag{33}$$

Therefore, from equation 33 the closed-loop transfer function for roll, pitch and yaw attitude control dynamics for the uncompensated system is as shown in equation 34.

$$\left.\begin{aligned}\frac{\theta_{a1}(s)}{\theta_{r1}(s)} &= \frac{A_1}{s^4+Bs^3+Cs^2+Ds+A_1}\\ \frac{\theta_{a2}(s)}{\theta_{r2}(s)} &= \frac{A_2}{s^4+Bs^3+Cs^2+Ds+A_2}\\ \frac{\theta_{a3}(s)}{\theta_{r3}(s)} &= \frac{A_3}{s^4+Bs^3+Cs^2+Ds+A_3}\end{aligned}\right\} \tag{34}$$

The system general open-loop transfer function when PID controller was incorporated into the system was obtained from equation 31 and is as shown in equation 35.

$$\frac{\theta_{ai}(s)}{V_{ei}(s)} = \frac{A_iK_Ds^2+A_iK_Ps+A_iK_I}{s^5+Bs^4+Cs^3+Ds^2} \tag{35}$$

From equation 35 the open-loop transfer function for roll, pitch and yaw PID attitude-controlled dynamics is as shown in equation 36.

$$\left.\begin{aligned}\frac{\theta_{a1}(s)}{V_{e1}(s)} &= \frac{A_1K_Ds^2+A_1K_Ps+A_1K_I}{s^5+Bs^4+Cs^3+Ds^2}\\ \frac{\theta_{a2}(s)}{V_{e2}(s)} &= \frac{A_2K_Ds^2+A_2K_Ps+A_2K_I}{s^5+Bs^4+Cs^3+Ds^2}\\ \frac{\theta_{a3}(s)}{V_{e3}(s)} &= \frac{A_3K_Ds^2+A_3K_Ps+A_3K_I}{s^5+Bs^4+Cs^3+Ds^2}\end{aligned}\right\} \tag{36}$$

From equation 35 the general closed-loop transfer function for the PID controlled system is as expressed in equation 37.

$$\frac{\theta_{ai}(s)}{\theta_{ri}(s)} = \frac{A_iK_Ds^2+A_iK_Ps+A_iK_I}{s^5+Bs^4+Cs^3+(A_iK_D+D)s^2+A_iK_Ps+A_iK_I} \tag{37}$$

Therefore, from equation 37 the closed-loop transfer function for roll, pitch and yaw PID controlled attitude dynamics is as shown in equation 38.

$$\left.\begin{aligned}\frac{\theta_{a1}(s)}{\theta_{r1}(s)} &= \frac{A_1K_Ds^2+A_1K_Ps+A_1K_I}{s^5+Bs^4+Cs^3+(A_iK_D+D)s^2+A_iK_Ps+A_iK_I}\\ \frac{\theta_{a2}(s)}{\theta_{r2}(s)} &= \frac{A_2K_Ds^2+A_2K_Ps+A_2K_I}{s^5+Bs^4+Cs^3+(A_iK_D+D)s^2+A_iK_Ps+A_iK_I}\\ \frac{\theta_{a3}(s)}{\theta_{r3}(s)} &= \frac{A_3K_Ds^2+A_3K_Ps+A_3K_I}{s^5+Bs^4+Cs^3+(A_iK_D+D)s^2+A_iK_Ps+A_iK_I}\end{aligned}\right\} \tag{38}$$

3 SYSTEM SIMULATION

To enhance the understanding and analysis of system behaviour, the system subunits and the overall system response to unit step test signal were simulated using Matlab software. The weight and physical dimension of the satellite of Figure 1 are M = 30kg, $l_1 = 0.4$m, $l_2 = 0.4$m, $l_3 = 0.3$m. By substituting the value of M, l_1, l_2 and l_3 into equation 5, the numerical value for J_1, J_2 *and* J_3 was found to be 0.625 kgm^2, 0.625 kgm^2 and 0.800 kgm^2 respectively. Also, the transfer functions for the satellite structure dynamics along the roll, pitch and yaw axis were obtained by substituting the value of J_1, J_2 *and* J_3 into equation 4 and these transfer functions were used to plot the step response of Figure 4.

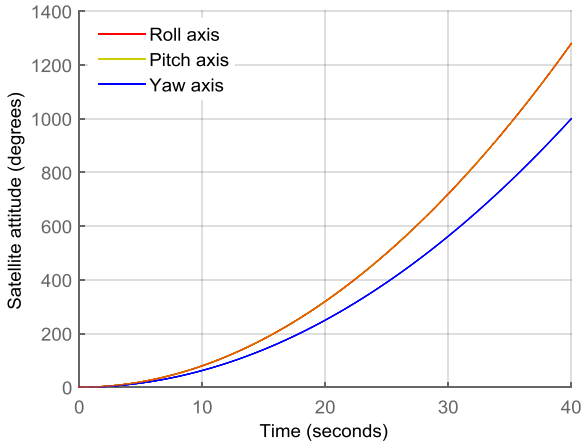

Figure 4. Step response for satellite structure dynamic model

From the table of parameters and units of Maxon motor [24] and equations 17 and 18, the following values were obtained: $K = 37.5940$, $T_m = 0.0142$s and T_e =0.00046667s. Also, from equation 22 assuming the angular speed of the motor to be equal that of the wheel, the wheel moments of inertial J_{w1}, J_{w2} and J_{w3} were obtained to be 0.00010935kgm^2, 0.00010935kgm^{2}and 0.00013997kgm^{2}respectively. Substituting these parameters value into equation 25 yielded the reaction wheel transfer function for roll, pitch and yaw axis respectively. The step function response for these transfer functions is as shown in Figure 5.

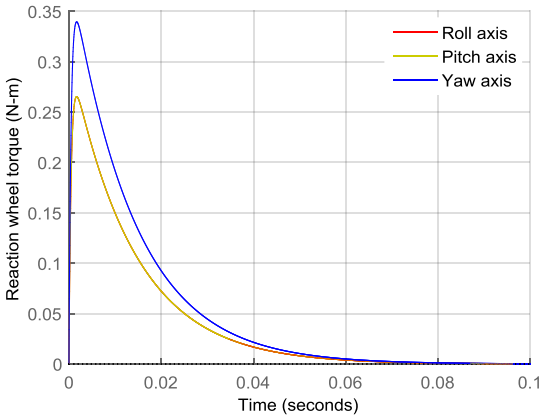

Figure 5. Step response for reaction wheel dynamic model

For the selected Maxon motor the value of V_a is 12V, assuming the maximum value of V to be 0.1V, therefore at steady state using equation 27 we have $K_{amp} = 120$. Let the amplifier settling time be 1second, then $\tau_{amp} = 0.25$ second. By substituting the value of K_{amp} and τ_{amp} obtained into equation 26, the amplifier transfer function was obtained and the step response for this transfer function is as shown in Figure 6.

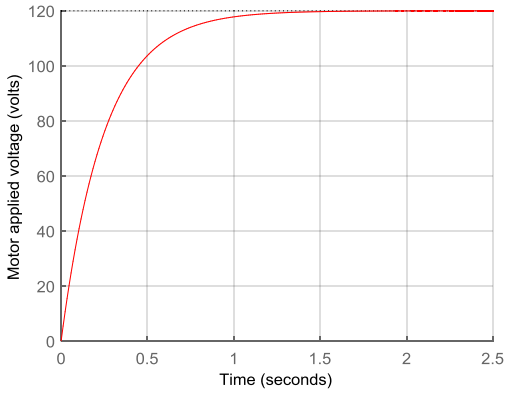

Figure 6. Step response for amplifier model

The system open-loop and closed-loop transfer function for roll, pitch and yaw axis was obtained by substituting the determined values of the wheel, motor and amplifier parameters into equations 32 and 34 respectively. And the system open-loop and closed-loop step response are as shown in Figures 7 and 8 respectively.

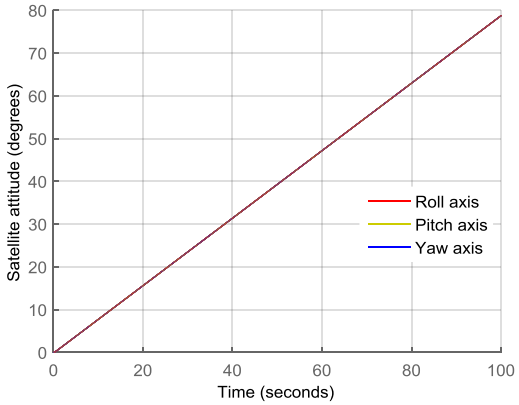

Figure 7. Step response for uncontrolled system open-loop transfer function

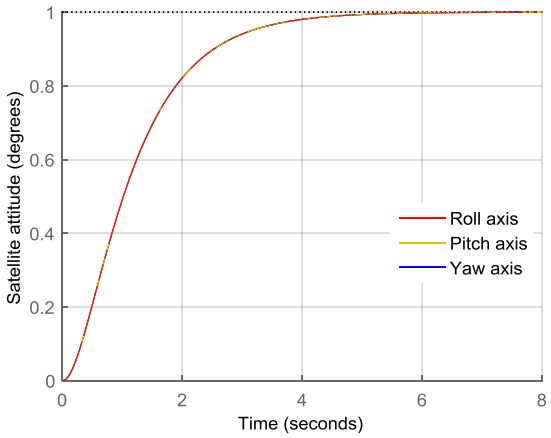

Figure 8. Step response for uncontrolled system closed-loop transfer function

4 RESULTS AND DISCUSSION

Considering Figure 4 the satellite dynamic structure response to step input for the roll and pitch axes are the same because the satellite has the same physical dimensions along these axes. It can also be observed from Figure 4 that the satellite structure dynamic model is an unstable sub-system because the only two existing poles for this sub-system transfer function are located at the origin in the *s* plane. Figure 5 is the response of the reaction wheel dynamic model to a step function input. It can be seen clearly from equation 25 that this sub-system is a second-order, but the response of Figure 5 does not conform to that of the standard second-order system due to presence of the system zero

which is located at the origin in the s plane. The response of Figure 6 shows that the amplifier dynamic is of first-order as already proposed in equation 25. More so, the system time-domain performance parameters of the amplifier sub-system are: T_r= 0.549s, T_s= 0.978s, PO=0 and E_{ss}=0. The percentage error between the obtained and assumed settling time is 2.2% which is okay. The steady-state peak amplitude of 120 was obtained when the time was 2.5s, thereby confirming the conformity of the calculated amplifier gain and the obtained value from the response graph. It can be seen from Figure 7 that the system is open-loop unstable. The responses for the roll, pitch and yaw axes are the same because of the effect of the difference in satellite and wheel moment of inertial for the roll, pitch and yaw axes have cancelled out as the ratio of these two parameters are the same for each of the axes. Figure 8 shows that the system is closed-loop stable and the time domain parameters obtained for the roll, pitch and yaw axes are the same (T_r=2.21s, T_s=3.98s, PO= 0 and E_{ss}=0). The responses for the three axes are the same because of the reason given for the system open-loop responses since the system closed-loop transfer function is a function of its open-loop transfer function. From simulation, the system reaches the peak maximum value of unity when the time $\geq$ 8s.

5 CONCLUSIONS

The microsatellite attitude control subsystems were modelled and subsequently used to develop the overall system model. The developed models were simulated using the system step response. The simulation results showed that the uncompensated system is open-loop unstable but closed-loop stable with T_r= 2.21s, T_s= 3.98s, PO= 0 and E_{ss} = 0 for all the three axes. The system performance can further be improved by designing an appropriate PID controller using the proposed models.

REFERENCES

1. Bohari, B., Ismail, L.N.M. and Varatharajoo, R. (2007). Spacecraft pitch and roll/yaw actuations using control moment gyroscopes for attitude stabilization. *Jurnal Mekanikal,* vol. 23, no.23, pp. 1-14.

2. Saberi, F.F., Fazlyab, A. and Ajorkar, A. (2014). Design and Implementation of a Sliding Mode Attitude Controller of a Satellite in Software in the Loop Test Bed. *International Journal of Computer Applications*, vol. 98, no. 16, pp. 28-34.

3. Dorf, R.C. and Bishop, R.H. (2010).Modern control systems. Upper Saddle River, NJ: Prentice Hall, pp. 148-151.

4. Shi, K., Liu, C. and Sun, Z. (2016). Mixed H2/H∞ State Feedback Attitude Control of Microsatellite Based on Extended LMI Method. *Journal of Harbin Institute of Technology*, vol. 23, pp. 15-22.

5. Xiao, B., Huo, M. Yang, X. and Zhang, Y. (2015). Fault-tolerant attitude stabilization for satellites without rate sensor. *IEEE Transactions on Industrial Electronics,* vol. 62, no. 11, pp. 7191-7202.

6. Xiao, B., Hu, Q., Wang, D. and Poh, E.K. (2013). Attitude tracking control of rigid spacecraft with actuator misalignment and fault. *IEEE Transactions on Control Systems Technology,* vol. 21, no. 6, pp. 2360-2366.

7. Bustan, D., Sani, S.H. and Pariz, N. (2013). Adaptive fault-tolerant spacecraft attitude control design with transient response control. *IEEE/ASME Transactions on Mechatronics*, vol. 19, no. 4, pp. 1404-1411.

8. Yu, Y. and Yang, Z. (2016). A semi-physical simulation platform of attitude determination and control system for satellite. *Advances in Mechanical Engineering,* vol. 8, no. 5, pp. 1-11.

9. Mehedi, M. and Filipski, M.N. (2005). Design of a momentum bias attitude control system with a double reaction wheel assembly. *Ankara International Aerospace Conference, Ankara, Turkey*, pp. 1-8.

10. Liu, C., Sun, Z., Shi, K. and Wang, F. (2018). Robust non-fragile state feedback attitude control for uncertain spacecraft with input saturation. *Proceedings of the Institution of Mechanical Engineers, Part G: Journal of Aerospace Engineering,* vol. 232, no. 2, pp. 246-259.

11. Pinheiro, E.R. and De Souza, L.C.G. (2013). Design of the Microsatellite Attitude Control System Using the Mixed Method via LMI Optimization. *Mathematical Problems in Engineering,* pp. 1-8.

12. Wu, B., Cao, X. and Li, Z. (2009). Multi-objective output-feedback control for microsatellite attitude control: An LMI approach. *Acta Astronautica,* vol. 64, nos. 11-12, pp. 1021-1031.

13. Santana, A.C., Martins-Filho, L.S., Duarte, R.O., Arantes Jr, G. and Casella, I.S. (2012). Attitude Control of a Satellite by Using Digital Signal Processing. *Journal of Aerospace Technology and Management,* vol. 4, no.1, pp. 15-24.

14. Mahdi, M.C. and Shehab, A.R. (2014). Attitude Determination and Control System design of KufaSat. *International Journal of Current Engineering and Technology,* vol. 4, no. 4, pp. 2910-2920.

15. Molina, J.C., Ayerdi, V. and Zea, L. (2016). Attitude Control Model for CubeSats. *Techn Session VII: Attitude Determination and Control Systems*, pp. 1-22.

16. Mbaocha, C.C., Eze, C.U., Ezenugu, I.A. and Onwumere, J.C. (2016). Satellite Model for Yaw-Axis Determination and Control Using PID Compensator. *International Journal of Scientific & Engineering Research,* vol. 7, no. 7, pp. 1623-1629.

17. Ar-Ramahi, S.K.H. (2009). PID controller design for the satellite attitude control system. *Journal of Engineering,* vol. 15, no. 1, pp. 3312-3320.

18. Shou, H.N. (2014). Micro-satellite Attitude Determination and Control Subsystem Design and Implementation: Software-in-the-Loop Approach. *International Symposium on Computer, Consumer and Control*, pp. 1283-1286.

19. Vatel, R. and Sinclair, D. (2012). Comparison of Control Moment Gyros and Reaction Wheels for Small Earth-Observing Satellites. *26th Annual AIAA/USU Conference on Small Satellites,* pp. 1-7.

20. Mohsenipour, R., Nemati, H., Nasirian, M. and Nia, A.K. (2013). Attitude control of a flexible satellite by using robust control design methods. *Intelligent Control and Automation,* vol. 4, no. 3, pp. 313-326.

21. Xu, B., Wang, X., Xiang, C., Ma, Y. and Chen, W. (2015). Modelling and hovering control of a novel multi-tandem ducted fan vehicle. *International Conference on Unmanned Aircraft Systems (ICUAS)*, pp. 1346-1354.

22. Patel, V.K.S. and Pandey, A. (2013). Modeling and performance analysis of PID controlled BLDC motor and different schemes of PWM controlled BLDC motor. *International Journal of Scientific and Research Publications,* vol. 3, no. 4, pp. 1-14.

23. Sumayya, N., Laila, B.M. and Johnson, Y. (2016). Robust Reaction Wheel Attitude Control of Satellites. *International Journal of Scientific & Engineering Research,* vol. 7, no. 4, pp. 599-608.

24. Singh, S.K., Katal, N. and Modani, S. (2014). Optimization of PID controller for brushless DC motor by using Bio-inspired algorithms. *Research Journal of Applied Sciences, Engineering and Technology,* vol. 7, no. 7, pp. 1302-1308.